Journal of Energy Storage 115 (2025) 115997

Contents lists available at ScienceDirect

Journal of Energy Storage

journal homepage: www.elsevier.com/locate/est

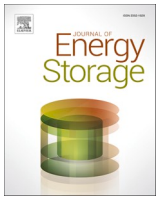

Research papers

Medium-entropy $Li_{1.2}Ni_{0.13}Co_{0.13}Mn_{0.54}O_2$ cathode with enhanced electrochemical performance by microstructural stabilization and surface modification

Zidong Zhou [a,1], Tongde Wang [a,1], Abdul Mateen [a], Jiawen Li [a], Xiang Chen [a], Wei Yan [a], Altaf Mujear [a], Yinfei Shao [a], Jing Chen [a], Xuesong Wang [a], Chengbin Liu [a], Guohua Gao [a,*], Yongfeng Mei [b,c,d,e], Guangming Wu [a], Zhihao Bao [a,*]

[a] School of Physics Science and Engineering, Tongji University, Shanghai 200092, China
[b] Yiwu Research Institute of Fudan University, Yiwu 322000, China
[c] Department of Materials Science & State Key Laboratory of Molecular Engineering of Polymers, Fudan University, Shanghai 200438, China
[d] Shanghai Frontiers Science Research Base of Intelligent Optoelectronics and Perception, Institute of Optoelectronics, Fudan University, Shanghai 200438, China
[e] International Institute of Intelligent Nanorobots and Nanosystems, Fudan University, Shanghai 200438, China

ARTICLE INFO

Keywords:
Mn-based materials
Mg/Al/La co-doping
Lithium-ion batteries
Li-rich cathode
DFT calculations

ABSTRACT

Lithium-rich layered oxides have gained considerable attention as cathode materials for lithium-ion batteries due to their high energy density. However, their insufficient structural stability results in rapid capacity fading and low initial Coulombic efficiency, hindering practical applications. In this study, we successfully synthesized medium-entropy $Li_{1.2}Ni_{0.13}Co_{0.13}Mn_{0.54}O_2$ (LMNCO) through co-doping with Mg, Al, and La. The optimized $Li_{1.2}Ni_{0.12}Co_{0.12}Mn_{0.53}Mg_{0.01}Al_{0.01}La_{0.01}O_2$ exhibited outstanding electrochemical performance, including a high initial reversible capacity of 272 mAh g^{-1}, an initial Coulombic efficiency of 82.2 %, and a capacity retention of 83 % after 100 cycles. These improvements can be attributed to the microstructural advantages, including optimized lattice parameters, enhanced lattice oxygen stability, and strengthened transition metal-oxygen bonds. Density functional theory (DFT) calculations further confirmed that Mg, Al, and La co-doping increased the adsorption energy (−3.12 eV) and the number of transferred electrons (0.87 e) compared with samples doped with each element individually. Meanwhile, the p-band center energy level of oxygen at the lithium adsorption site increased, further verifying that medium entropy facilitated the enhancement of electrochemical performance. The co-doping method suggests a promising strategy to develop cathode materials with enhanced capacity and stability, designed for the next generation of lithium-ion batteries.

1. Introduction

With the rapidly growing demand for high energy density and environmental sustainability in lithium-ion batteries (LIBs) [1], significant efforts have been dedicated to improving the electrochemical performance of lithium-rich ternary oxides (LRTOs) [2]. Li-rich manganese-based oxides (LRMOs) demonstrate outstanding properties, such as a specific capacity exceeding 300 mAh g^{-1}, a mean discharge voltage more than 3.5 V, and cost-effective [3,4]. However, structural instability, the key problem for LRMOs, still results in capacity degradation, reduced cycle-stability, and low Coulombic efficiency [5–7].

To address the structural instability and other related issues of LRMOs, several approaches have been proposed, including the morphological and structural design of electrode materials [8,9], elemental doping with Na, K, Mg, Cs, and Ru [10–14], surface coatings [15–18], and combinations of the above approaches [19–23]. For instance, Huang et al. [24] synthesized magnesium-doped LRTOs, where the Mg dopant acted as a stabilizing agent, improving reversible capacity. Similarly, the use of aluminum doping has been examined to hinder the transition to the spinel phase in $Li_{1.2}Ni_{0.16}Mn_{0.51}Al_{0.05}Co_{0.08}O_2$ [25]. Therefore, Mg and Al doping improve electrochemical performance. In addition, they are cost-effective, widely available, and

* Corresponding authors.
E-mail addresses: gao@tongji.edu.cn (G. Gao), zbao@tongji.edu.cn (Z. Bao).
[1] These authors contributed equally to this work and should be considered co-first authors.

https://doi.org/10.1016/j.est.2025.115997
Received 2 January 2025; Received in revised form 14 February 2025; Accepted 23 February 2025
Available online 27 February 2025

environmentally friendly. La doping has also gained attention due to its ability to form unique La—O bond with both ionic and relatively covalent properties, which enhanced the stability of lattice oxygen and expanded the reversibility of oxygen redox reactions [26]. While numerous previous works have focused on single-element doping, co-doping studies have also shown promise. For example, the co-doping of Fe and Cl has been shown to reduce the irreversible release of lattice oxygen, mitigate voltage fading, and enhance initial Coulombic efficiency [27]. Similarly, Ce and B co-doping combined with CeO_2 surface coating on $Li_{1.184}Ni_{0.136}Co_{0.136}Mn_{0.544}O_2$ were used to solve irreversible anion redox limits [7]. Moreover, doping can also increase the entropy of electrode materials, providing a novel pathway for enhancing electrochemical performance. Ding et al. [28] observed the increased interlayer spacing in high-entropy materials contributed to strengthening the overall skeletal structure of layered oxides by alleviating Jahn-Teller distortion effects [29,30]. Likewise, medium-entropy doping involving multiple ions has been shown to enhance the stability of high-voltage cathode materials [31,32]. Unfortunately, the existing doping techniques still fall short in achieving a concurrent enhancement in discharge capacity, cycle retention rate, and initial Coulombic efficiency. Furthermore, to enhance the electrochemical performance of the material, we introduced a Li_2WO_4 (LWO) coating on the medium-entropy material. The primary role of the Li_2WO_4 coating is to stabilize the material's surface, reducing side reactions between the electrolyte and the electrode material, thereby improving the cycling stability of the material. Although the Li_2WO_4 coating is not entirely consistent with the medium-entropy strategy, its synergistic effect with the medium-entropy material can significantly enhance the electrochemical performance. Therefore, by combining the medium-entropy strategy with surface coating technology, we have designed a cathode material with superior electrochemical performance.

In view of the stabilization effect of Mg, Al, and La in LRMOs cathode, we propose replacing the M (M = Ni, Co, Mn) ions in $Li_{1.2}Ni_{0.13}Co_{0.13}Mn_{0.54}O_2$ (LMNCO) with small amounts of above elements to obtain the co-doped one ($Li_{1.2}Ni_{0.12}Co_{0.12}Mn_{0.53}Mg_{0.01}Al_{0.01}La_{0.01}O_2$, D-LMNCO), which also simultaneously increases its entropy. Compared with unmodified LMNCO, D-LMNCO demonstrates improved electrochemical performance, with an initial capacity of 272 mAh g^{-1}, a Coulombic efficiency of 82.2 %, and capacity retention of 83 % after 100 cycles, benefiting from the enhancements in its microstructure. Furthermore, the application of a Li_2WO_4 coating further enhances the electrochemical performance of D-LMNCO, resulting in a composite material (C-D-LMNCO) with an initial capacity of 284 mAh g^{-1}, a Coulombic efficiency of 85.0 %, and capacity retention of 90.2 % after 100 cycles. Undoubtedly, these combined modification methods were the basis for the design of stable LRMOs, which could be used to make high-caliber cathode materials and next-generation LIBs with improved stability and capacity retention.

2. Experimental methods

2.1. Material preparation

The $Li_{1.2}Ni_{0.12}Co_{0.12}Mn_{0.53}Mg_{0.01}Al_{0.01}La_{0.01}O_2$ (D-LMNCO) material was synthesized using a ball-milling-assisted oxalate precipitation method. Specifically, 2 mmol of manganese acetate, 0.5 mmol of cobalt acetate, and 0.5 mmol of nickel acetate were dissolved in a mixed solvent comprising deionized water, ethylene glycol, and ethanol in a Volumetric ratio of 1:1:4. After complete precipitation with 6 mmol of oxalic acid, the precipitate was pre-sintered at 500 °C for 6 h to yield the precursor material. This precursor was then subjected to ball milling in the presence of a 7 % excess of lithium carbonate and suitable quantities of magnesium acetate, aluminum oxide, and lanthanum acetate at 300 rpm for 6 h. Subsequently, the mixture underwent calcination in an air environment at 800 °C for 12 h, resulting in D-LMNCO. Meanwhile, in a ball milling system, when no additives are introduced, the resultant material is LMNCO, whereas, with the individual addition of suitable quantities of magnesium acetate, aluminum oxide, and lanthanum acetate as dopants, the materials are denoted as Mg-LMNCO, Al-LMNCO, and La-LMNCO, respectively. To prepare the coating solution, tungsten trioxide and lithium hydroxide monohydrate were dissolved and agitated at 60 °C for 15 h. The resulting mixture was dried, ground with D-LMNCO, and sintered to obtain the coated material, denoted as C-D-LMNCO.

2.2. Material characterization

The crystalline structures of the synthesized materials were analyzed by powder X-ray diffraction (XRD) using Cu Kα radiation on a Rint-2000 diffractometer (Rigaku, Japan). The diffraction patterns were acquired over a 2θ range of 10–70° with a step size of 0.02°. The crystallographic parameters were analyzed using MDI Jade 5.0 software. Morphological characterization of the prepared materials was conducted using scanning electron microscopy (SEM, JSM-6510) and high-resolution transmission electron microscopy (HRTEM, JEM-2100, JEOL, Japan). The atomic concentrations of Ni, Co, Mn, Mg, Al, La, and W in the materials were accurately quantified using inductively coupled plasma optical emission spectroscopy (ICP-OES). Furthermore, X-ray photoelectron spectroscopy (XPS) was used to elucidate the oxidation states of the individual metal elements within the co-doped materials.

2.3. Electrochemical measurements

A slurry was prepared by combining the active material, polyvinylidene fluoride (PVDF), and carbon black in an *N*-methyl-2-pyrrolidone solvent at a weight ratio of 80:10:10. The slurry was subsequently applied to aluminum foil and dried in a vacuum oven at 80 °C for 12 h. The dried foil was cut into disks, each possessing a mass loading of approximately 2 mg/cm^2, to act as the working electrode. The electrochemical performance was assessed using a coin cell (CR-2016) constructed within an argon-filled glovebox (LG1200/750TS; Vigor, China). Lithium metal foil served as the counter electrode, accompanied by a porous polymer separator (Celgard 2400) and a 1 M $LiPF_6$ electrolyte solution composed of a 1:1 volume ratio of ethylene carbonate (EC) and dimethyl carbonate (DMC). Galvanostatic charge-discharge tests were performed at ambient temperature utilizing a battery testing system (LAND, 2001 T, China) within a voltage range of 2.0–4.6 V (vs. Li/Li^+). Cyclic Voltammetry (CV) measurements were conducted utilizing an electrochemical workstation (Autolab 302 N), across a potential range of 2 to 4.6 V vs. Li/Li^+, at a scan rate of 0.1 mV/s. Electrochemical impedance spectroscopy (EIS) was conducted on a three-electrode setup utilizing an electrochemical workstation (Autolab 302 N) across a frequency spectrum of 0.01 Hz to 100 kHz, with a 5 mV AC perturbation signal applied. In this configuration, the working electrode was previously used, whereas the lithium foil and lithium ring served as the counter and reference electrodes, respectively.

2.4. Calculation method

All calculations were conducted using the Vienna Ab-initio Simulation Package (VASP, version 6.4.1) employing the projector-augmented wave (PAW) method [33,34]. A truncation energy of 520 eV and an energy convergence criterion of $1E^{-6}$ with a mechanical convergence criterion of −0.03 are used in the calculations to ensure that the energy error is lower than 1 meV/atom. A 5 × 5 × 2 k-point network is used for structural optimization, and 8 × 8 × 3 network is used for the density of states calculations.

3. Results and discussion

XRD analysis was used to investigate the structural characteristics of LMNCO, Mg-LMNCO, Al-LMNCO, La-LMNCO, D-LMNCO, and C-D-

LMNCO. As illustrated in Fig. 1a, the XRD patterns display a characteristic hexagonal α-$NaFeO_2$ layered structure corresponding to the R3¯m space group. All the main diffraction peaks in the pattern can be well-matched with the hexagonal $LiTMO_2$ phase (space group: R3¯m, JCPDS#09-0063). The several weak diffraction peaks in the 20–25°range are caused by the Li/Mn - ordered superlattice structure in the transition - metal layer, which is a typical structural feature of the monoclinic Li_2MnO_3 phase (space group: C2/m, JCPDS#84-1634). The distinct separation of the (006)/(102) and (108)/(110) peaks confirms the systematic layering structure of both the pristine and doped samples, hence validating their characteristic hexagonal layered structures. Combined with the ICP results (Table S1), the elemental proportions of all samples are in accordance with the designed values, which also indicates that we have successfully prepared these materials. Fig. 1b, c show that the (003) and (104) peaks of all the doped samples shift to lower diffraction angles, indicating an expansion in the Li slab dimension. This shift to lower diffraction angles and the expansion in the Li slab dimension are because the different ionic radii of dopants (Mg, Al, La) compared to the original cations expand the lattice, especially along the c-axis related to Li-layer spacing. Table S2, which summarizes the statistics from Fig. 1d-f, illustrate that the a and c lattice parameters of D-LMNCO increase from 2.8471 Å and 14.2132 Å (LMNCO) to 2.8522 Å and 14.2511 Å, respectively [35]. Meanwhile, the enhanced intensity ratio of (003)/(104) and the c/a ratio indicates that D-LMNCO effectively reduced cation mixing [36].The results indicate that the doping approach effectively enlarges the spacing between the Li layers, which is critical for facilitating Li - ion migration across the oxide layers during lithiation and delithiation processes and ultimately improving electrochemical performance.

The scanning electron microscopy (SEM) images of LMNCO (Fig. 2a), D-LMNCO (Fig. 2b), and C-D-LMNCO (Fig. 2c) show that all samples exhibit well-defined spindle-shaped particles. Significantly, SEM images at the scale of 200 nm of LMNCO (Fig. 2d), D-LMNCO (Fig. 2e), and C-D-LMNCO (Fig. 2f) illustrate that LMNCO, D-LMNCO possess similar surface structures with only marginal differences. Meanwhile, the surface of C-D-LMNCO displays increased densification after modification, indicating improved interparticle bonding [37]. High-resolution transmission electron microscopy (HRTEM) images (Fig. 2g-i) of LMNCO, D-LMNCO, and C-D-LMNCO reveal lattice fringes in the interior regions, with spacings of 4.78 Å, 4.68 Å, and 4.69 Å, aligned well with spacings of the (003) plane of the R3¯m phase and the (001) plane of the C2/m phase [38], respectively. The HRTEM image of C-D-LMNCO (Fig. 2i) clearly shows that the LWO coating layer in C-D-LMNCO is approximately 10–20 nm.

To better understand the surface structure and element valence distribution, XPS was performed. As shown in Fig. 3a-c and Fig. S2, Ni, Co, Mn, Mg, Al, La and W spectrum demonstrate remarkable consistency with relevant literature. Notably, the spectrum of La^{3+} bears a certain resemblance to that of Ni^{2+}, which accounts for the observable coalescence of partial peaks in Fig. 3a. Moreover, the coating process is prone to attenuate the peak intensities, as manifested by the evidently diminished peak intensities of the C-D-LMNCO spectrum in Fig. 3a-c in comparison to LMNCO and D-LMNCO [25,26,39]. Furthermore, Fig. 3d-f show that the binding energy of lattice oxygen (O^{2-}) in C-D-LMNCO (529.59 eV) is higher than that in LMNCO (529.45 eV), which suggests stronger TM-O bonds on the surface of C-D-LMNCO. This is due to the W—O bond's higher dissociation energy than the Mn—O, Ni—O, and Co—O bonds on C-D-LMNCO [40]. This modification enhances structural stability by increasing the binding energy of surface lattice oxygen and mitigating the irreversible release of surface lattice oxygen. Enhancing the stability of lattice oxygen is considered an effective approach for achieving improved electrochemical performance in LIBs. Additionally, Fig. 3g-i illustrate that after co-doping with Mg, Al, and La, the proportion of lattice oxygen (at 529.5 eV) increases from 48.41 % to 56.16 %. The peaks at 531.2 eV and 532.0 eV correspond to O—H species and carbonate moieties, respectively. The suppressive effect of dopant modification on the irreversible release of lattice oxygen may be associated with the optimization of the local environment of oxygen. Typically, the local environment of oxygen is primarily composed of O—H species, carbonate groups, and lattice oxygen. The presence of O—H species and carbonate groups significantly affect the surface stability of lithium-rich layered oxides. This phenomenon can induce a structural transition from the layered phase to a spinel-like phase morphology, thereby reducing cycling stability. Additionally, it generates oxygen vacancies, which impede the re-insertion of the Li^+ ions to the lattice structure [41]. Therefore, D-LMNCO is expected to exhibit

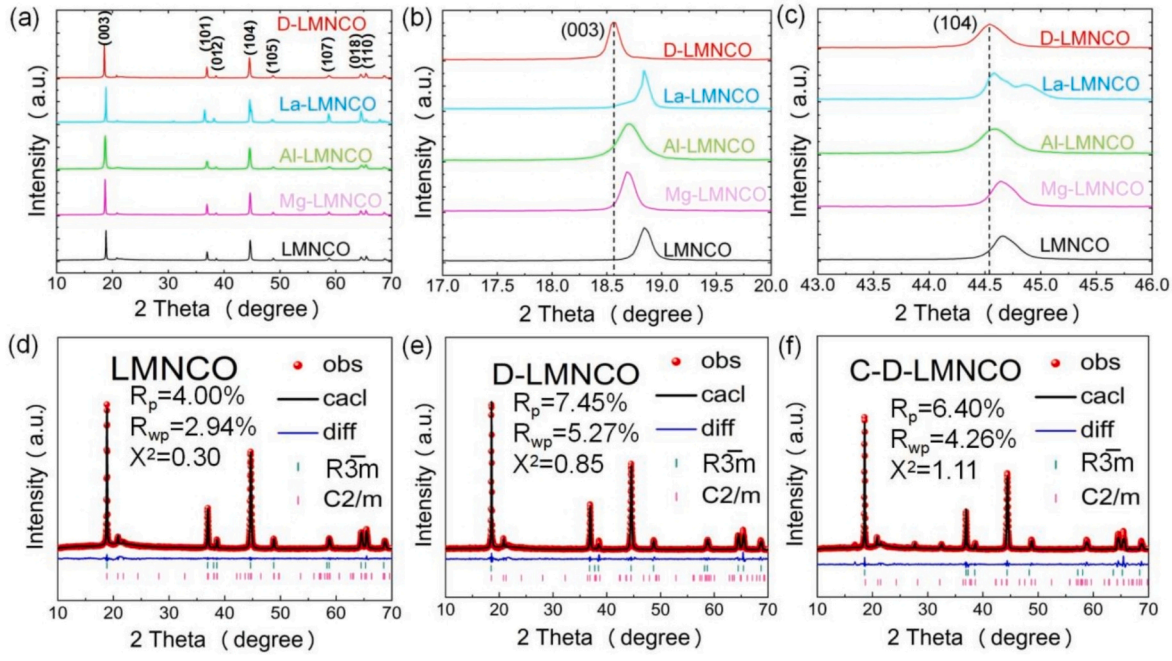

Fig. 1. (a)XRD patterns of samples, enlarged views of the (003) peak (b) and (104) peak (c), Rietveld refinement XRD patterns for (d) LMNCO, (e) D-LMNCO, and (f) C-D-LMNCO samples.

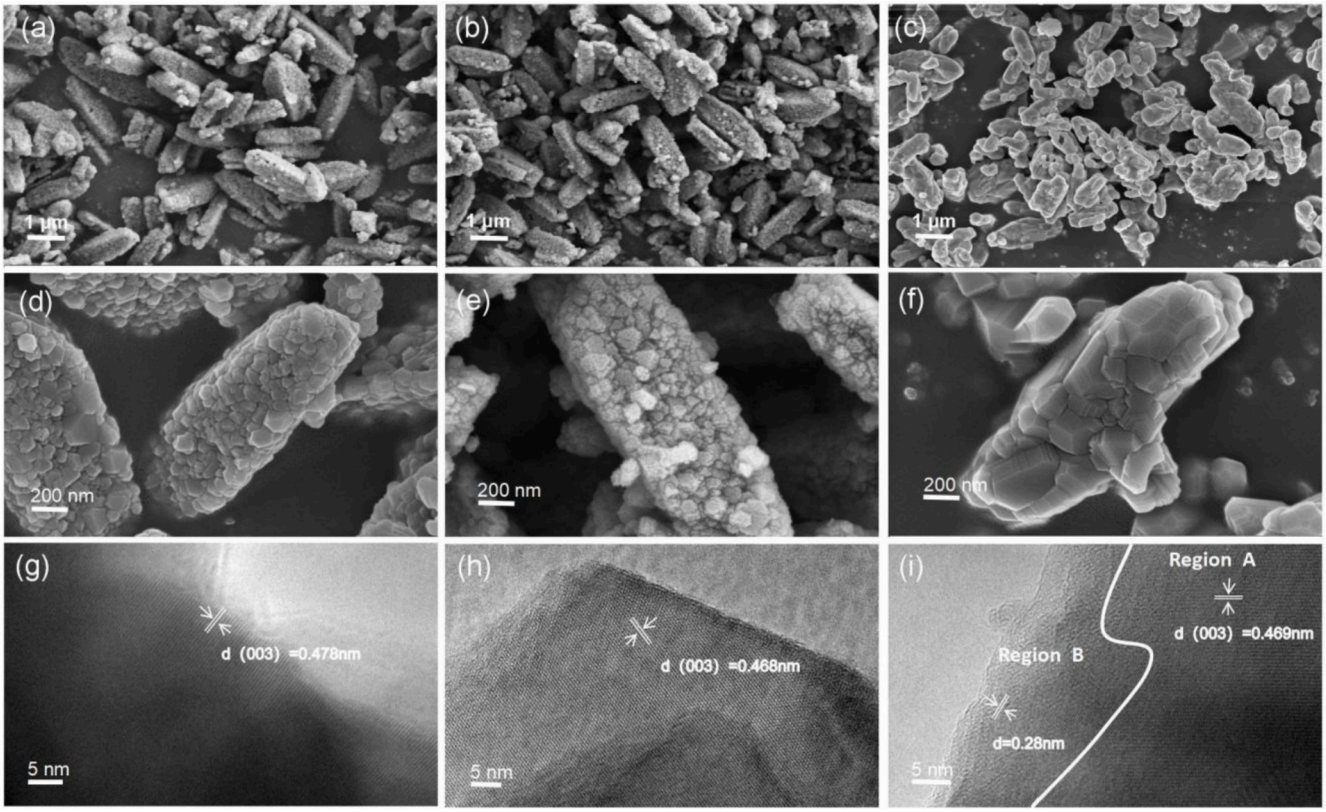

Fig. 2. SEM images of (a, d) LMNCO, (b, e) D-LMNCO, (c, f) C-D-LMNCO at different magnifications, and HRTEM images of (g) LMNCO, (h) D-LMNCO, and (i) C-D-LMNCO.

superior electrochemical performance due to better environment of oxygen.

A comprehensive investigation of the crystal structure and morphology confirms the effective introduction of Mg, Al, and La elements into the lattice structure by the co-doping method. This doping process fails to result in noticeable changes in the morphology or crystalline structure of the materials. To clarify the relationship between the mixed doping protocol, the structural characteristics of the material, and its performance metrics, the electrochemical properties of the electrode materials were evaluated using a half-cell configuration, with LMNCO, D-LMNCO, and C-D-LMNCO working as cathodes with lithium foil anodes. Fig. 4a illustrates that LMNCO presents a discharge capacity of 251 mAh g^{-1}, accompanied by an initial Coulombic efficiency of 79.4 %. Upon doping, D-LMNCO exhibits an enhanced discharge capacity of 272 mAh g^{-1} and an initial coulombic efficiency reaching 82.2 %. These enhancements can be attributed to the co-doping of Mg, Al, and La, which synergistically improve lattice oxygen stability and increase lithium-ion adsorption energy. Electrode materials' performance in energy storage systems is significantly influenced by their surface properties and ion-transfer kinetics. The cathode-electrolyte interface often suffers from side reactions that lead to the consumption of active materials and lithium ions, thus deteriorating the overall performance. A fast-ion-conductor coating can act as a protective layer and a facilitator for ion transfer. Li_2WO_4, as a fast-ion-conductor, has unique characteristics. It has a relatively high lithium-ion conductivity, which can effectively optimize the lithium-ion intercalation kinetics during the charge-discharge process. By coating the medium-entropy material with Li_2WO_4, a more stable interface between the electrode and the electrolyte can be created. This not only suppresses the side reactions at the cathode-electrolyte interface but also accelerates the transfer of lithium ions, which is crucial for enhancing the material's discharge capacity and Coulombic efficiency. Although it may not seem directly related to the medium-entropy strategy in terms of elemental composition, its function in improving the overall electrochemical performance is complementary. As shown in our experimental results, the discharge capacity of C-D-LMNCO is enhanced to 284 mAh g^{-1}, with its initial coulombic efficiency reaching 85 %, which is largely attributed to the LWO coating. Additionally, Fig. 4a also depicts the initial charge-discharge curves of Mg-LMNCO, Al-LMNCO and La-LMNCO. As shown in Table S3, La doping modestly enhanced the capacity while significantly improving the coulombic efficiency, whereas Mg and Al doping contributed to minor increments in discharge capacity. As illustrated in Fig. 4b, the D-LMNCO cathode demonstrates commendable capacities of 271.2, 223.1, 193.8, 159.4, 127, and 92 mAh g^{-1} at current densities of 0.1, 0.5, 1, 2, 5, and 10C, respectively. Therefore, D-LMNCO exhibits a substantial rate of performance compared to the LMNCO cathode. Moreover, both D-LMNCO and C-D-LMNCO demonstrate pronounced advantages at higher current rates, underscoring their enhanced kinetic properties. In addition, Fig. 4c shows the cycling stability tests of LMNCO, D-LMNCO, and C-D-LMNCO conducted at 1.0C. The LMNCO exhibits a retention of 80.5 % of its capacity after 100 cycles. In contrast, D-LMNCO maintains 83 % of its capacity over the same period. Notably, C-D-LMNCO exhibits enhanced durability, retaining 90.2 % of its capacity after 100 cycles. Consequently, the co-doping of Mg, Al, and La exhibited enhanced electrochemical performance of LMNCO. The enhancements in initial discharge capacity, capacity retention throughout cycle, and initial Coulombic efficiency are due to increased structural stability., increased lithium-ion adsorption energy, and increased entropy, validating the efficacy of the doping strategy.

EIS was performed to LMNCO, D-LMNCO, and C-D-LMNCO to clarify reaction processes and interfacial electrochemistry. The following equation calculates lithium-ion diffusion coefficient [42].

$$Z' = R_s + R_{ct} + \sigma\omega^{-0.5} \quad (1)$$

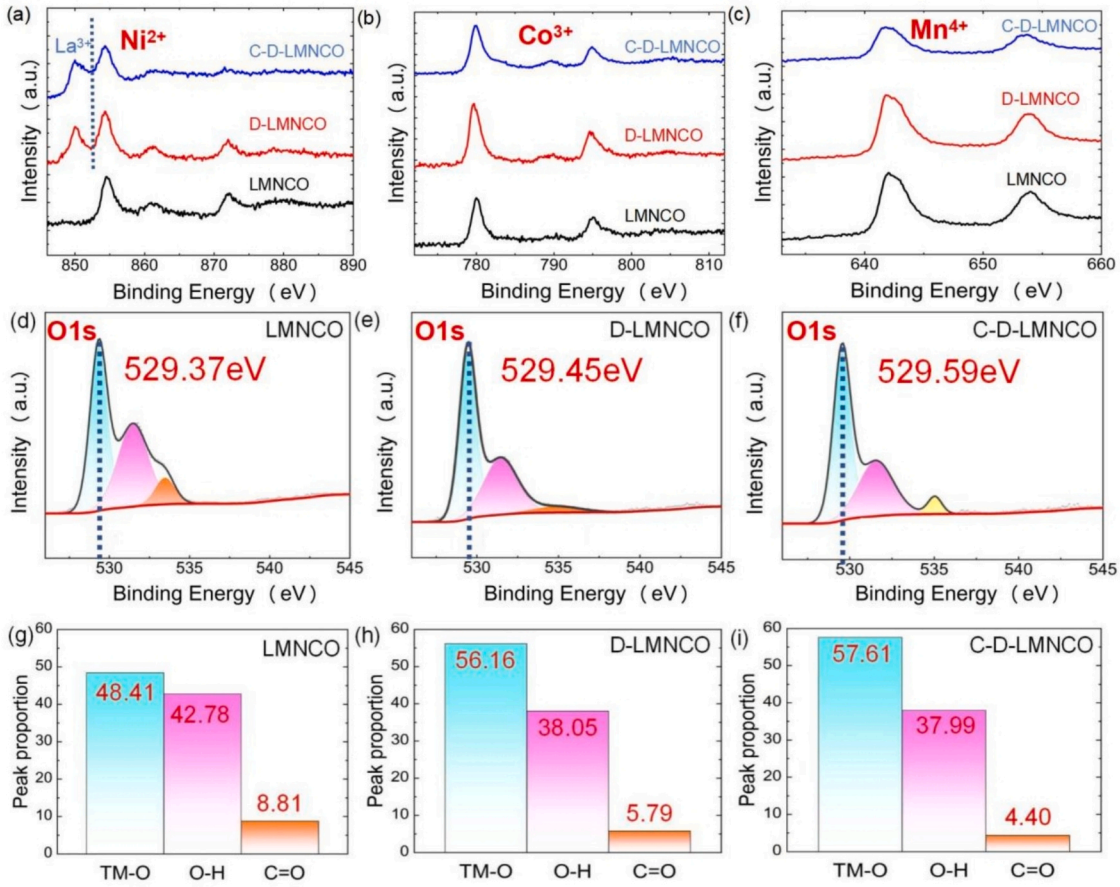

Fig. 3. High-resolution XPS spectra of (a) Ni 2p, (b) Co 2p, (c) Mn 2p for LMNCO, D-LMNCO, C-D-LMNCO, and O1s for (d) LMNCO, (e) D-LMNCO, and (f) C-D-LMNCO samples; peak intensities of O1s for (g) LMNCO, (h) D-LMNCO, and (i) C-D-LMNCO samples.

$$D_{Li^+} = 0.5\left(\frac{RT}{AF^2\sigma wC}\right)^2 \quad (2)$$

In the above equations, the angular frequency is denoted by ω, whereas R, T, F and A represent the gas constant, absolute temperature, Faraday's constant and the electrode surface area, respectively. Fig. 4d, e exhibited a slope at low frequencies and a semicircle at high frequencies, indicative of diffusion and charge transfer processes, respectively. The corresponding values for uncompensated ohmic resistance (R_s), charge transfer resistance (R_{ct}), Warburg impedance (W), and constant phase element (CPE) Q were calculated using Zsimpwin software and are summarized in Table S4 [22,36]. As presented in Table S4, C-D-LMNCO exhibits the highest D_{Li^+}, which may be attributed to the enlarged interlayer distance and shortened diffusion pathways facilitated by the combined doping of Mg, Al, and La. Additionally, the optimized doping and surface coating strategies significantly reduced the R_{ct} value, indicating enhanced conductivity and improved kinetics of Li insertion and extraction. The potential difference (ΔE_p) between the O_1 oxidation peak and R_2 reduction peak in the CV curves serves as an indicator of electrode polarization [43]. As shown in Fig. 4f-h, C-D-LMNCO displayed a ΔE_p value of 0.62 V, which is lower than the values of approximately 0.68 V for D-LMNCO and 0.69 V for LMNCO after three cycles, which indicates the reduced polarization of C-D-LMNCO during cycling. Consequently, reduced polarization facilitates enhanced Li^+ transport across the coating layer interface, in combination with delayed structural transformation from layered to spinel phase, resulting in low-capacity degradation and improved electrochemical performance of the infused specimen [44,45]. Notably, we compared the electrochemical performance of LMNCO, Mg-LMNCO, D-LMNCO, and C-D-LMNCO samples (Fig. 4i). Both D-LMNCO and C-D-LMNCO exhibited superior performance concerning D_{Li^+}, capacity, and the Coulombic efficiency.

To investigate the effect of doping on oxide-embedded lithium, we constructed a model for DFT calculations based on the XRD and TEM results (Fig. S3). Fig. 5a depicts the distribution of electrons at the doping sites of the oxide material during elemental doping. From blue to red, it represents a gradual increase in the number of electrons. It can be observed that elements Mn and Ni have a higher number of electrons, while the number of electrons at the sites decreases when Mg/Al/La is doped. The doping of several elements together results in a state of electron deficiency at the site. As shown in Fig. 5b, the electron exchange between lithium atoms and the electrode material during insertion. The oxygen atom acts as an anchor point during insertion and directly exchanges electrons with the Li atom. The electrons flow from the Li atom to the O atom, resulting in electrostatic adsorption to form a bond. It is clearly seen that there is electron flow between Mn and O, while it is not obvious between Mg/Al/La and O. Fig. 5c shows the adsorption energy of Li atoms upon insertion, versus the corresponding number of electrons exchanged with the electrode material. Doping effectively increases the adsorption energy of Li atoms, which represents an increase in the adsorption strength and macroscopically favors the increase in the performance of the electrode materials. There is a positive correlation between the electron exchange number and the adsorption energy. From Fig. 5a, b, it can be found that due to the state of electron deficiency at the doped sites, it leads to a weaker bonding with the O atoms. The O atoms is more inclined to obtain electrons from the inserted Li atoms to form bonds, which effectively increases the adsorption strength of the Li atoms.

The density-of-states diagrams before and after Li insertion was calculated, from which the positions of the P-band centers of the O elements with different models, as well as the bonding after Li insertion

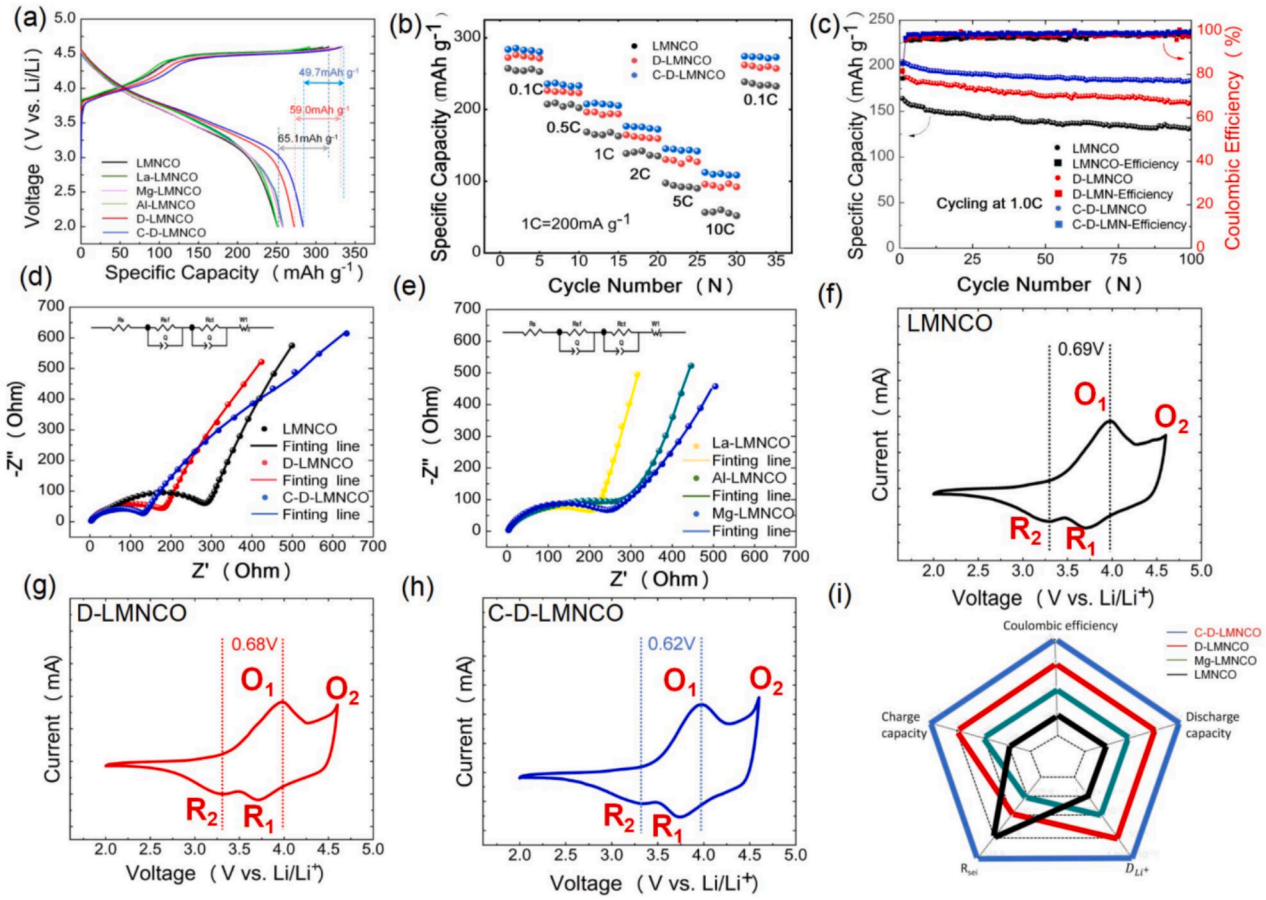

Fig. 4. Electrochemical performances of the half-cells. (a)First charge and discharge curves at 0.1C. (b) Rate capability. (c) Cycling performance. (d) Nyquist plots of the samples. (e)Nyquist plots of the half-cells using La-LMNCO, Mg-LMNCO, and Al-LMNCO sample. The third CV curve for the pristine LMNCO (f), D-LMNCO (g), and C-D-LMNCO (h). Comparison of the electrochemical performance (i).

are obtained, which are plotted as Fig. 5d. It can be seen that the doping of different elements successfully affects the electronic properties of the O atoms. The increase of the P-band centers leads to an increase in the heights of the antibonding orbitals formed with the Li atoms, which represents an increase of the adsorption strength, and this corresponds to the adsorption energy results. Finally, Fig. 5e shows the overall effect of doping elements on the density of states of the electrode material. The doping element mainly affects the state density distribution of O rather than the formation of impurity states directly at the Fermi energy level. These results comprehensively illustrate the influence mechanism of doping on the electronic structure and properties of the electrode material from multiple perspectives.

4. Conclusion

In summary, co-doping with Mg, Al, and La was employed to modify the microstructure and improve the electrochemical performance of the material… The synergistic effect of doping increased entropy, optimized the lattice parameters, and mitigated polarization. DFT calculations demonstrated that the incorporation of Mg, Al, and La elevates the p-band center energy level of O at the Li adsorption site and increases the antibonding orbitals that form upon adsorption. Thus, the bonding affinity with Li atoms was bolstered and the adsorption energy was augmented. Consequently, the initial discharge capacity and Coulombic efficiency of D-LMNCO were 272 mAh g^{-1} and 82.2 %, respectively, with a capacity retention of 83 % after 100 cycles. Subsequently, after coating LWO onto the surface of the material, C-D-LMNCO demonstrated a superior performance, achieving an initial discharge capacity of 284 mAh g^{-1} and a Coulombic efficiency of 85.0 % at a rate of 0.1C, and a remarkable capacity retention of 90.2 % after 100 cycles at 1C. Such co-doping and entropy-enhancing approach significantly enhanced the electrochemical properties of the material, providing a practical and effective method to increase the microstructural stability of additional layered metal oxides for use in LIBs. This work provides valuable insights for the advancement of high-performance cathode materials for future LIBs.

CRediT authorship contribution statement

Zidong Zhou: Writing – review & editing, Writing – original draft, Methodology, Investigation, Formal analysis, Data curation, Conceptualization. **Tongde Wang:** Validation, Software, Formal analysis, Data curation, Conceptualization. **Abdul Mateen:** Writing – original draft, Visualization, Validation, Conceptualization. **Jiawen Li:** Methodology, Formal analysis, Data curation. **Xiang Chen:** Methodology, Investigation, Conceptualization. **Wei Yan:** Investigation, Formal analysis, Conceptualization. **Altaf Mujear:** Validation, Formal analysis. **Yinfei Shao:** Methodology, Investigation, Conceptualization. **Jing Chen:** Formal analysis, Conceptualization. **Xuesong Wang:** Methodology, Formal analysis, Conceptualization. **Chengbin Liu:** Investigation, Formal analysis, Data curation. **Guohua Gao:** Writing – review & editing, Writing – original draft, Formal analysis, Conceptualization. **Yongfeng Mei:** Writing – review & editing, Writing – original draft, Investigation, Formal analysis. **Guangming Wu:** Visualization, Validation, Formal analysis. **Zhihao Bao:** Writing – review & editing, Writing – original draft, Visualization, Validation, Supervision, Formal analysis.

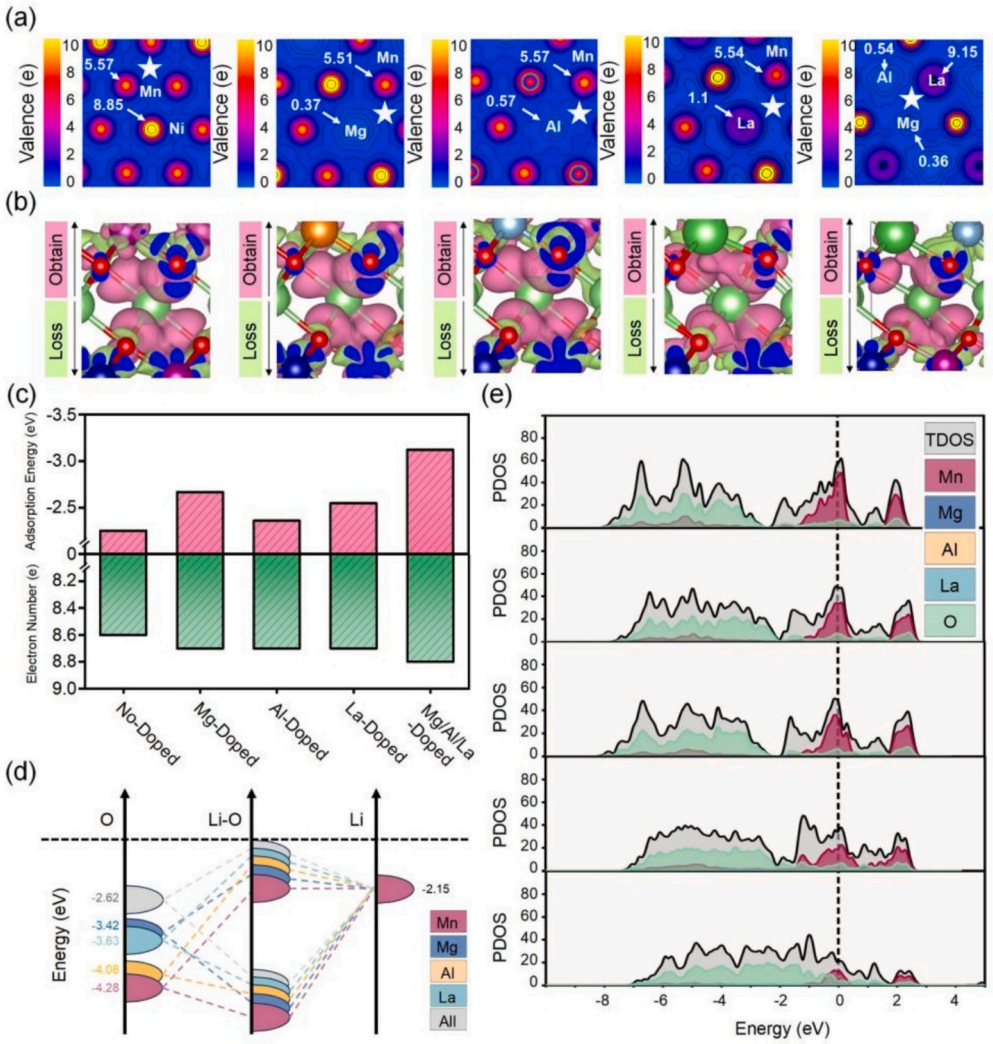

Fig. 5. Effect of doping elements on (a) electron distribution, (b) differential charge upon Li embedding, (c) adsorption energy and electron exchange number, (d) matching of P-band centers of O atoms to Li atoms upon adsorption, and (e) density of states.

Author statement

We declare that this manuscript is original, has not been published before and is not currently being considered for publication elsewhere.

We confirm that the manuscript has been read and approved by all named authors and that there are no other persons who satisfied the criteria for authorship but are not listed. We further confirm that the order of authors listed in the manuscript has been approved by all of us.

We understand that the Corresponding Author is the sole contact for the Editorial process. He is responsible for communicating with the other authors about progress, submissions of revisions and final approval of proofs.

Declaration of competing interest

The authors declare that they have no known competing financial interests or personal relationships that could have appeared to influence the work reported in this paper.

Acknowledgments

This study was supported by the National Natural Science Foundation of China (Grant No. 52378217), the research fund from Shanghai Key Laboratory of Special Artificial Microstructure Materials and Technology.

Zidong Zhou and Tongde Wang (hereinafter referred to as Z.Z. and T.W.) gratefully acknowledge Xiang Chen, Wei Yan, Jiawen Li, Altaf Mujeara, Yinfei Shao, Jing Chen, Xuesong Wang, Chengbin Liu, Guohua Gao, Yongfeng Mei, Zhihao Bao, and Abdul Mateen for their invaluable contributions. Specifically, Z.Z. and T.W. thank Xiang Chen, Wei Yan, and Jiawen Li for their assistance in understanding the intricacies of the research problem; Altaf Mujeara, Yinfei Shao, and Jing Chen for their insightful discussions on experimental methodologies; and Xuesong Wang, Chengbin Liu, and Abdul Mateen for their expert guidance on technical aspects.

Additionally, Z.Z. and T.W. express their sincere gratitude to Professor Zhihao Bao for his multifaceted support, and to Professor Guohua Gao and Professor Yongfeng Mei for their crucial contributions, respectively.

Appendix A. Supplementary data

Supplementary data to this article can be found online at https://doi.org/10.1016/j.est.2025.115997.

Data availability

Data will be made available on request.

References

[1] H.-Y. Jang, D. Eum, J. Cho, J. Lim, Y. Lee, J.-H. Song, H. Park, B. Kim, D.-H. Kim, S.-P. Cho, et al., Structurally robust lithium-rich layered oxides for high-energy and long-lasting cathodes, Nature Communications 15 (1) (2024), https://doi.org/10.1038/s41467-024-45490-x.

[2] Y. Yang, C. Gao, T. Luo, J. Song, T. Yang, H. Wang, K. Zhang, Y. Zuo, W. Xiao, Z. Jiang, et al., Unlocking the potential of Li-rich Mn-based oxides for high-rate rechargeable lithium-ion batteries, Adv. Mater. 35 (52) (2023), https://doi.org/10.1002/adma.202307138.

[3] Z. Liu, Y. Zeng, J. Tan, H. Wang, Y. Zhu, X. Geng, P. Guttmann, X. Hou, Y. Yang, Y. Xu, et al., Revealing the degradation pathways of layered Li-rich oxide cathodes, Nat. Nanotechnol. (2024), https://doi.org/10.1038/s41565-024-01773-4.

[4] Q. Jiang, X. Li, Y. Hao, J. Zuo, R. Duan, J. Li, G. Cao, J. Wang, J. Wang, M. Li, et al., Oxygen-vacancy-assisted dual functional surface coatings suppressing irreversible phase transition of Li-rich layered oxide cathodes, Adv. Funct. Mater. (2024), https://doi.org/10.1002/adfm.202400670.

[5] W. Zeng, F. Xia, J. Wang, J. Yang, H. Peng, W. Shu, Q. Li, H. Wang, G. Wang, S. Mu, et al., Entropy-increased $LiMn_2O_4$-based positive electrodes for fast-charging lithium metal batteries, Nature Communications 15 (1) (2024), https://doi.org/10.1038/s41467-024-51168-1.

[6] Y.S. Jiang, Z.M. Liao, F.D. Yu, W. Ke, X.Y. Li, Y. Xia, G.J. Xu, G. Sun, Y.G. Xia, W. Yin, et al., A cable-stayed honeycomb superstructure to improve the stability of Li-rich materials via inhibiting interlaminar lattice strain, Adv. Mater. (2024) 36 (31), https://doi.org/10.1002/adma.202404982.

[7] S. Kang, X. Wei, Y. Chu, Y. Mu, L. Zou, X. Xu, Q. Zhang, L. Zeng, Simultaneous dual modification of Li-rich Mn-based cathode in restraining oxygen release and structure distortion, J. Mater. Chem. A 12 (16) (2024) 9584–9593, https://doi.org/10.1039/d4ta00483c.

[8] T. Wu, X. Liu, X. Zhang, Y. Lu, B. Wang, Q. Deng, Y. Yang, E. Wang, Z. Lyu, Y. Li, et al., Full concentration gradient-tailored Li-rich layered oxides for high-energy lithium-ion batteries, Adv. Mater. 33 (2) (2020), https://doi.org/10.1002/adma.202001358.

[9] X. Ji, Q. Xia, Y. Xu, H. Feng, P. Wang, Q. Tan, A review on progress of lithium-rich manganese-based cathodes for lithium ion batteries, J. Power Sources (2021) 487, https://doi.org/10.1016/j.jpowsour.2020.229362.

[10] S. Chen, Z. Chen, M. Xia, C. Cao, Y. Luo, Toward alleviating voltage decay by sodium substitution in lithium-rich manganese-based oxide cathodes, ACS Applied Energy Materials 1 (8) (2018) 4065–4074, https://doi.org/10.1021/acsaem.8b00740.

[11] Q. Li, G. Li, C. Fu, D. Luo, J. Fan, L. Li, K^+-doped $Li_{1.2}Mn_{0.54}Co0_{.13}Ni_{0.13}O_2$: a novel cathode material with an enhanced cycling stability for lithium-ion batteries, ACS Appl. Mater. Interfaces 6 (13) (2014) 10330–10341, https://doi.org/10.1021/am5017649.

[12] X. Jin, Q. Xu, H. Liu, X. Yuan, Y. Xia, Excellent rate capability of Mg doped Li $[Li_{0.2}Ni_{0.13}Co_{0.13}Mn_{0.54}]O_2$ cathode material for lithium-ion battery, Electrochim. Acta 136 (2014) 19–26, https://doi.org/10.1016/j.electacta.2014.05.043.

[13] X. Ding, Y.-X. Li, M.-M. Deng, S. Wang, Y. Aqsa, Q. Hu, C.-H. Chen, Cesium doping to improve the electrochemical performance of layered $Li_{1.2}Ni_{0.13}Co_{0.13}Mn_{0.54}O_2$ cathode material, J. Alloys Compd. 791 (2019) 100–108, https://doi.org/10.1016/j.jallcom.2019.03.297.

[14] B. Song, M.O. Lai, L. Lu, Influence of Ru substitution on Li-rich $0.55Li_2MnO_3{\cdot}0.45LiNi_{1/3}Co_{1/3}Mn_{1/3}O_2$ cathode for Li-ion batteries, Electrochim. Acta 80 (2012) 187–195, https://doi.org/10.1016/j.electacta.2012.06.118.

[15] F. Zheng, C. Yang, X. Xiong, J. Xiong, R. Hu, Y. Chen, M. Liu, Nanoscale surface modification of Lithium-rich layered-oxide composite cathodes for suppressing voltage fade, Angew. Chem. Int. Ed. 54 (44) (2015) 13058–13062, https://doi.org/10.1002/anie.201506408.

[16] S. Kim, W. Cho, X. Zhang, Y. Oshima, J.W. Choi, A stable lithium-rich surface structure for lithium-rich layered cathode materials, Nature Communications 7 (1) (2016), https://doi.org/10.1038/ncomms13598.

[17] Y. Xie, S. Chen, W. Yang, H. Zou, Z. Lin, J. Zhou, Improving the rate capability and decelerating the voltage decay of Li-rich layered oxide cathodes by constructing a surface-modified microrod structure, J. Alloys Compd. 772 (2019) 230–239, https://doi.org/10.1016/j.jallcom.2018.09.046.

[18] H. Zhang, T. Yang, Y. Han, D. Song, X. Shi, L. Zhang, L. Bie, Enhanced electrochemical performance of $Li_{1.2}Ni_{0.13}Co_{0.13}Mn_{0.54}O_2$ by surface modification with the fast lithium-ion conductor Li-La-Ti-O, J. Power Sources 364 (2017) 272–279, https://doi.org/10.1016/j.jpowsour.2017.08.050.

[19] Y. Liu, S. Zheng, Q. Wang, Y. Fu, H. Wan, A. Dou, V.S. Battaglia, M. Su, Improvement the electrochemical performance of Cr doped layered-spinel composite cathode material Li 1.1 Ni 0.235 $Mn_{0.735}Cr_{0.03}O_{2.3}$with $Li_4T_5O_{12}$ coating, Ceram. Int. 43 (12) (2017) 8800–8808, https://doi.org/10.1016/j.ceramint.2017.04.011.

[20] Z. Tai, W. Zhu, M. Shi, Y. Xin, S. Guo, Y. Wu, Y. Chen, Y. Liu, Improving electrochemical performances of Lithium-rich oxide by cooperatively doping Cr and coating Li_3PO_4 as cathode material for Lithium-ion batteries, J. Colloid Interface Sci. 576 (2020) 468–475, https://doi.org/10.1016/j.jcis.2020.05.015.

[21] Y. Liu, X. Fan, Z. Zhang, H.-H. Wu, D. Liu, A. Dou, M. Su, Q. Zhang, D. Chu, Enhanced electrochemical performance of Li-rich layered cathode materials by combined Cr doping and $LiAlO_2$ coating, ACS Sustain. Chem. Eng. 7 (2) (2018) 2225–2235, https://doi.org/10.1021/acssuschemeng.8b04905.

[22] C. Shen, Y.Q. Liu, W.R. Li, X.Y. Liu, J.W. Xie, J.L. Jiang, Y. Jiang, B. Zhao, J. J. Zhang, One-pot synthesis and multifunctional surface modification of lithium-rich manganese-based cathode for enhanced structural stability and low-temperature performance, J. Colloid Interface Sci. 615 (2022) 1–9, https://doi.org/10.1016/j.jcis.2022.01.176.

[23] M. Li, Y. Zhou, X. Wu, L. Duan, C. Zhang, F. Zhang, D. He, The combined effect of CaF_2 coating and La-doping on electrochemical performance of layered lithium-rich cathode material, Electrochim. Acta 275 (2018) 18–24, https://doi.org/10.1016/j.electacta.2018.04.077.

[24] Y.Y. Huang, Y.C. Zhu, H.Y. Fu, M.Y. Ou, C.C. Hu, S.J. Yu, Z.W. Hu, C.T. Chen, G. Jiang, H.K. Gu, et al., Mg-pillared $LiCoO_2$: towards stable cycling at 4.6 V, Angewandte Chemie-International Edition 60 (9) (2021) 4682–4688, https://doi.org/10.1002/anie.202014226.

[25] P.K. Nayak, J. Grinblat, M. Levi, E. Levi, S. Kim, J.W. Choi, D. Aurbach, Al doping for mitigating the capacity fading and voltage decay of layered Li and Mn-rich cathodes for Li-ion batteries, Advanced Energy Materials 6 (8) (2016). DOI: 10.1002/aenm.201502398.

[26] Z. Liu, Y. Wu, H. Huo, J. Jian, D. Sun, X. Zhang, C. Du, P. Zuo, G. Yin, Y. Ma, Surface-phase engineering via lanthanum doping enables enhanced electrochemical performance of Li-rich layered cathode, ACS Applied Energy Materials 5 (8) (2022) 9648–9656, https://doi.org/10.1021/acsaem.2c01295.

[27] L. Nie, Z. Wang, X. Zhao, S. Chen, Y. He, H. Zhao, T. Gao, Y. Zhang, L. Dong, F. Kim, et al., Cation/anion codoped and cobalt-free Li-rich layered cathode for high-performance Li-ion batteries, Nano Lett. 21 (19) (2021) 8370–8377, https://doi.org/10.1021/acs.nanolett.1c02923.

[28] K. Walczak, A. Plewa, C. Ghica, W. Zając, A. Trenczek-Zając, M. Zając, J. Toboła, J. Molenda, $NaMn_{0.2}Fe_{0.2}Co_{0.2}Ni_{0.2}Ti_{0.2}O_2$ high-entropy layered oxide – experimental and theoretical evidence of high electrochemical performance in sodium batteries, Energy Storage Materials 47 (2022) 500–514, https://doi.org/10.1016/j.ensm.2022.02.038.

[29] F. Ding, C. Zhao, D. Xiao, X. Rong, H. Wang, Y. Li, Y. Yang, Y. Lu, Y.-S. Hu, Using high-entropy configuration strategy to design Na-ion layered oxide cathodes with superior electrochemical performance and thermal stability, J. Am. Chem. Soc. 144 (18) (2022) 8286–8295, https://doi.org/10.1021/jacs.2c02353.

[30] Z. Lun, B. Ouyang, D.-H. Kwon, Y. Ha, E.E. Foley, T.-Y. Huang, Z. Cai, H. Kim, M. Balasubramanian, Y. Sun, et al., Cation-disordered rocksalt-type high-entropy cathodes for Li-ion batteries, Nat. Mater. 20 (2) (2020) 214–221, https://doi.org/10.1038/s41563-020-00816-0.

[31] X.-Y. Feng, W.-T. Wu, Q.-Q. Huang, Y.-C. Liu, C. Ni, Z.-M. Huang, X. Liang, C.-H. Chen, H.-F. Xiang, Medium entropy stabilized disordered $LiNi_{0.5}Mn_{1.5}O_4$ cathode with enhanced electrochemical performance, J. Alloys Compd. (2023) 948, https://doi.org/10.1016/j.jallcom.2023.169768.

[32] W. Wu, S. Zuo, X. Zhang, X. Feng, Two-step solid state synthesis of medium entropy $LiNi_{0.5}Mn_{1.5}O_4$ cathode with enhanced electrochemical performance, Batteries 9 (2) (2023), https://doi.org/10.3390/batteries9020091.

[33] G. Kresse, Efficient iterative schemes for ab initio total-energy calculations using a plane-wave basis set, Phys. Rev. B 6 (1) (July 1996) 15–50.

[34] G. Kresse, From ultrasoft pseudopotentials to the projector augmented-wave method, Phys. Rev. B 59 (3) (1998) 1758–1775.

[35] R. Zhang, C. Wang, P. Zou, R. Lin, L. Ma, T. Li, I.-H. Hwang, W. Xu, C. Sun, S. Trask, et al., Long-life lithium-ion batteries realized by low-Ni, Co-free cathode chemistry, Nature Energy 8 (7) (2023) 695–702, https://doi.org/10.1038/s41560-023-01267-y.

[36] M. Yoon, Y. Dong, Y. Huang, B. Wang, J. Kim, J.-S. Park, J. Hwang, J. Park, S. J. Kang, J. Cho, et al., Eutectic salt-assisted planetary centrifugal deagglomeration for single-crystalline cathode synthesis, Nat. Energy 8 (5) (2023) 482–491, https://doi.org/10.1038/s41560-023-01233-8.

[37] Y. Liu, X. Fan, B. Luo, Z. Zhao, J. Shen, Z. Liu, Z. Xiao, B. Zhang, J. Zhang, L. Ming, et al., Understanding the enhancement effect of boron doping on the electrochemical performance of single-crystalline Ni-rich cathode materials, J. Colloid Interface Sci. 604 (2021) 776–784, https://doi.org/10.1016/j.jcis.2021.07.027.

[38] J. Chen, G. Zou, W. Deng, Z. Huang, X. Gao, C. Liu, S. Yin, H. Liu, X. Deng, Y. Tian, et al., Pseudo-bonding and electric-field harmony for Li-rich Mn-based oxide cathode, Adv. Funct. Mater. 30 (46) (2020), https://doi.org/10.1002/adfm.202004302.

[39] X. Han, R. Wu, G. Gao, J. Li, M. Fan, S. Wang, Y. Liu, S. Li, L. Lin, Y. Zhang, et al., Lattice and local electronic structure modulation enables ultra-long-life Li-rich cathode materials, ACS Energy Lett. 9 (7) (2024) 3219–3226, https://doi.org/10.1021/acsenergylett.4c00939.

[40] Q. Li, M. Fu, X. Qin, A. Song, Y. Fan, Z. Ma, G. Shao, A unique three-dimensional network double-core–shell structure S@MnO_2@MXene suppresses the shuttle effect in high-sulfur-content high-performance lithium-sulfur batteries, J. Colloid Interface Sci. 674 (2024) 805–812, https://doi.org/10.1016/j.jcis.2024.06.211.

[41] J.-L. Shi, J.-N. Zhang, M. He, X.-D. Zhang, Y.-X. Yin, H. Li, Y.-G. Guo, L. Gu, L.-J. Wan, Mitigating voltage decay of Li-rich cathode material via increasing Ni content for Lithium-ion batteries, ACS Appl. Mater. Interfaces 8 (31) (2016) 20138–20146, https://doi.org/10.1021/acsami.6b06733.

[42] S. Li, L. Yang, Z. Liu, C. Zhang, X. Shen, Y. Gao, Q. Kong, Z. Hu, C.-Y. Kuo, H.-J. Lin, et al., Surface Al-doping for compromise between facilitating oxygen redox and enhancing structural stability of Li-rich layered oxide, Energy Storage Materials 55 (2023) 356–363, https://doi.org/10.1016/j.ensm.2022.12.006.

[43] H.-X. Wei, Y.-D. Huang, L.-B. Tang, C. Yan, Z.-J. He, J. Mao, K. Dai, X.-W. Wu, J.-B. Jiang, J.-C. Zheng, Lithium-rich manganese-based cathode materials with highly

stable lattice and surface enabled by perovskite-type phase-compatible layer, Nano Energy (2021) 88, https://doi.org/10.1016/j.nanoen.2021.106288.
[44] M. Wang, L. Chen, M. Liu, Y. Chen, Y. Gu, Enhanced electrochemical performance of La-doped Li-rich layered cathode material, J. Alloys Compd. (2020) 848, https://doi.org/10.1016/j.jallcom.2020.156620.
[45] D. Luo, H. Xie, F. Tan, X. Ding, J. Cui, X. Xie, C. Liu, Z. Lin, Scalable nitrate treatment for constructing integrated surface structures to mitigate capacity fading and voltage decay of Li-rich layered oxides, Angew. Chem. Int. Ed. 61 (27) (2022), https://doi.org/10.1002/anie.202203698.